Applied Physics A (2022) 128:208
https://doi.org/10.1007/s00339-022-05348-9

Applied Physics A
Materials Science & Processing

Cr_2O_3 effect on the structure, optical, and radiation shielding properties of $Na_2B_4O_7$–SiO_2–CaO–Cr_2O_3 glasses

Kh. S. Shaaban[1] · Ateyyah M. Al-Baradi[2] · Atif Mossad Ali[3,4]

Received: 30 November 2021 / Accepted: 27 January 2022 / Published online: 16 February 2022

Abstract
$65Na_2B_4O_7$–$25SiO_2$–$(10-x)$ CaO–x Cr_2O_3 $x=(0\leq x\leq 5$ mol.%) glass system was synthesized and optical, structural, and radiation shielding characteristics are examined. The glass density increased as Cr_2O_3 was added, while the molar volume decreased. FT-IR bands are correlated with the vibrations of BO_3 and BO_4. Cr^{3+} appears to convert BO_3 into BO_4, according to preliminary FT-IR results. E_{opt} values are in the range of 2.57–3.31 eV. Increases in the E_{opt} can be linked to density and N_4 variation. (*Zeq*) increased then decreased as the incident photon energy increased with the replacement of CaO by Cr_2O_3. $\sum R$ enhances as the Cr_2O_3 content of the glasses increases. G 5 is a better absorber of fast neutron when the FNRC of glass samples is compared. For neutron attenuation applications, the glass sample G 5 is the best option.

Keywords Cr_2O_3 · FT-IR · UV–Vis–NIR spectroscopy · Radiation

1 Introduction

Kodama noticed that the stoichiometric ratio of a wide range of binary sodium borate glasses $Na_2B_4O_7$ is established BO_3 is transformed into BO_4 [1–4]. At this ratio, Na_2O surrounds the network, preventing the surrounding soft B_2O_3 from deforming [5–12]. SiO_2 incorporated into alkali borate glasses improved their radiation and UV transmittance. As a result, alkali borosilicate glasses show promise for incorporating a variety of modifying oxides [13–17]. In technology, borosilicate glasses are extremely important. High-mechanical-stability household and laboratory glasses, as well as high-performance optical glasses, are some of their applications [15, 18–20].

Oxide glasses doped with transition metal ions (TMI) have recently attracted a lot of attention due to their appealing combination of physical and chemical characteristics. In recent years, TMI-doped borate, phosphate, silicate, and borosilicate glasses have been investigated physically, optically, and radiationally [21–30]. Glasses with semiconducting properties, such as Cr_2O_3, CdO, CuO, and others, are known as (TMO) glasses. There has been a lot of focus in recent years on borosilicate glasses containing various TMO, such as CoO, NiO, V_2O_5, and Cr_2O_3 [4, 31].

TMO-based glasses, such as Cr_2O_3, also have appealing optical properties, making them ideal for use as nonlinear optical (NLO) materials. According to previous research, TMO-containing borosilicate glasses have a variety of intriguing physical, structural, radiation, and spectroscopic characteristics [16, 17, 32]. As a result of the above existing literature, we have expanded our investigations into TM in calcium borosilicate glasses. As a result, we've developed calcium borosilicate glasses in a variety of compositions with Cr_2O_3 substituted. The synthesized glasses are characterized using XRD, FT-IR, and UV–Vis–NIR spectroscopy. The optical of these glasses with the composition $65Na_2B_4O_7$–$25SiO_2$–$(10-x)$ CaO–x Cr_2O_3, $x=(0\leq x\leq 5$ mol.%) are investigated in this study. In addition to the aforementioned studies, photons, neutrons, characteristics of Cr^{3+} doped calcium borosilicate glasses will be investigated using theoretical code in this work.

✉ Kh. S. Shaaban
khamies1078@yahoo.com

[1] Department of Chemistry, Faculty of Science, Al - Azhar University, Assiut 71452, Egypt

[2] Department of Physics, College of Science, Taif University, P.O. Box 11099, Taif 21944, Saudi Arabia

[3] Physics Department, Faculty of Science, King Khalid University, Abha 61413, Saudi Arabia

[4] Department of Physics, Faculty of Science, Assiut University, Assiut 71516, Egypt

2 Materials and methodology

Glasses with the following composition were formed using the traditional melt-quench procedure: $65Na_2B_4O_7-25SiO_2-10CaO$, $65Na_2B_4O_7-25SiO_2-9CaO-1Cr_2O_3$, $65Na_2B_4O_7-25SiO_2-8CaO-2Cr_2O_3$, $65Na_2B_4O_7-25SiO_2-6CaO-4Cr_2O_3$, $65Na_2B_4O_7–25SiO_2–5CaO–5Cr_2O_3$. Starting materials for the fabrication of glasses included high purity (Aldrich) CaO (99.5%), Cr_2O_3 (99.9%), SiO_2 (99.5%), and $Na_2B_4O_7$ (99.5%). The mixtures were then homogenized using a magnetic stirrer for 10 min. Glass was melted at 1100 °C in a platinum crucible. A random error in the melting temperature is ±10 °C. The glasses were annealed at 375 °C for 2 h. To calculate densities in toluene, the Archimedes model was used. On a Perkin Elmer Frontier FT-IR measurements in the 400–1800 cm^{-1} range were obtained using the KBr procedure. A random error in the center of FT-IR bands was found as ± 2 cm^{-1}. To establish a baseline and correct for noise, spectrum software was used. The optical description of these glasses was obtained in the wavelength range of 250–2500 nm by (JASCO V-670, Japan). The absorption coefficient (α), optical bandgap ($E_{opt.}^{indir}$), and refractive index (n_D) were all calculated using absorption spectra. As physical parameters related to optical energy, the following physical parameters were calculated: molar refractivity R_m, molar polarizability $\propto_m$, reflection loss R_L, metallization M, electronegativity χ, electron polarizability $\propto°$, optical basicity $\wedge$, Bulk module (K) and glass transition temperature $\left(T_{g(thero.)}\right)$: $R_m = Vm\left(1-\sqrt{Eopt./20}\right), \propto_m = \left(\frac{3}{4\pi N}\right)R_m$. $R_L = \left(\frac{R_m}{Vm}\right)$ $M = 1-\frac{R_m}{Vm}$, $\chi = 0.2688E_{opt.}$ $\propto° = -0.9\chi + 3.5$ and $\wedge = -0.5\chi + 1.7, K_{th} = -478.93 + 200.13E_{opt.}$, $T_{g(thero.)} = -701.87 + 403.33E_{opt.}$ As physical parameters related to the refractive index n_D, R_m, $\propto_m$, $\propto_0^{2-}$, and Λ were calculated: R_m, $\propto_m$, $\propto_0^{2-}$, and Λ. $R_m = \langle n^2-1\,|n^2+2\rangle Vm$, $\propto_m (3|4\pi N)R_m, \propto_0^{2-} = \frac{[\frac{Vm}{2.52}\left(\frac{n^2-1}{n^2+2}\right)-\Sigma\propto_{cat}]}{N_o^{2-}}$, and $\Lambda = 1.67\left(1-\frac{1}{\propto_0^{2-}}\right)$.

Using the online version of the Phy-X/PSD software, the study's goal was met by calculating all effective parameters that judge the prepared glasses shielding effectiveness [33]. Z_{eq} predictable with $eq = \frac{Z1(logR2-logR)+Z2(logR-logR1)}{logR2-logR1}$, The following parameters were calculated for G–P fitting: $P = \frac{P1(logZ2-logZeq)+Z2(logZeq-logZ1)}{logZ2-logZ1}$, EABF and EBF were calculated using G–P fitting. $B(E,X) = 1+\frac{b-1}{K-1}(K^x-1)$ for $K \neq 1$, $B(E,X) = 1+(b-1)x$ $K = 1$ where $K(E,X) = cx^a + d\frac{\tanh\left(\frac{x}{Xk}-2\right)-\tanh(-2)}{1-\tanh(-2)}$ for x ≤ 40.[30] and [40]

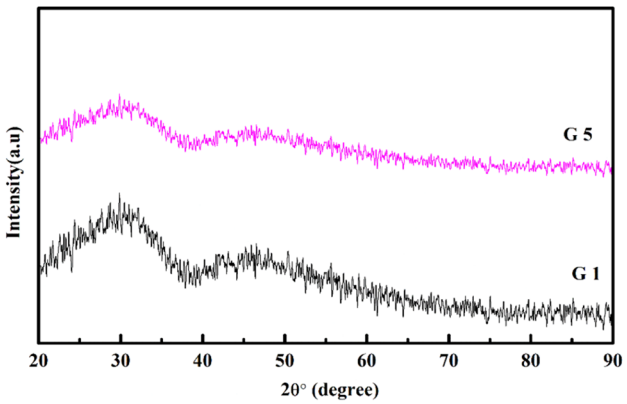

Fig. 1 XRD of synthetic glasses

3 Results and discussion

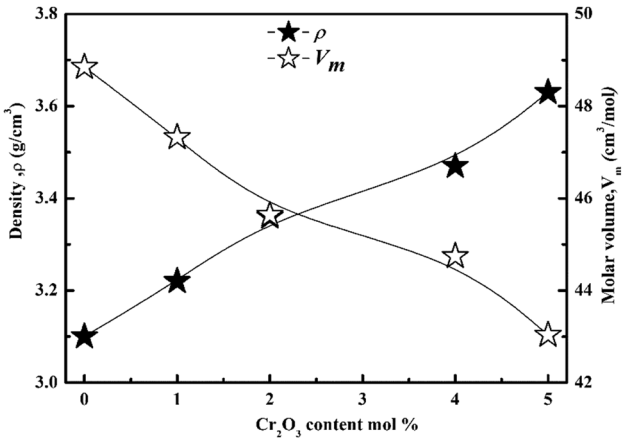

Fig. 2 ρ and V_m of synthetic samples

when Cr_2O_3 was added to them. The exchange of smaller CaO molecules (M = 56.077 g/mol, = 3.34 g/cm^3) with thicker and heavier Cr_2O_3 (M = 151.99 g/mol, = 5.2 g/cm^3) is the predominant cause of the increase in density. BO_3 have been transformed into BO_4 elements by the addition of modifier oxides like Cr_2O_3. The fact that BO_4 units are denser than BO_3 units demonstrates an increase in sample density [34, 37, 38].

3.2 FT-IR investigations

FT-IR spectrum of fabricating samples is exhibited in Fig. 3. In Fig. 3, the broad bands are the result of several distinct bands overlapping. Therefore, a deconvoluted process is used to obtain exact band positions. The difference between experimental and simulated Fig. is small than 0.02%. As a result, FT-IR of glasses was deconvoluted with (Peak Fit v4.12) using Gaussian distribution to determine the exact band positions and structural unit concentration.

Figure 4 depicts a typical glass deconvoluted FT-IR spectrum including band center (C), and relative area (A) as Table 1[8, 39–42]. (BO_3) is converted to (BO_4) in borosilicate glasses with low modifier oxide inclusions. For the borosilicate glasses, Si–O–B bonds must be established. The band at 442 cm^{-1} is combined with the deformation modes of the network structure. This band could be attributed to the cationic vibration of Ca-O in (CaO_6). The (NaO_6), (CrO_6), SiO_4, and Si–O–B vibrations are linked to bands in the 507–534 cm^{-1} range, which overlap with the O–Si–O. B–O–B bending vibrations of (BO_3) may be responsible for the bands observed at ~ 703 cm^{-1}. In borosilicate glasses with a large amount of alkaline earth oxides, SiO_4 tetrahedra with two NBOs can be found. Absorptions due to stretching vibrations of B–O–Si linkages between 952 and 1118 cm^{-1} must be noted, indicating a possible linkage between silicate and borate structural units [45]. The bands of 1000–1080 cm^{-1} due to the vibrations of the asymmetric stretching vibrations of Si–O–Si, O–Si–O^- [5]. The broadband between 836 and 1118 cm^{-1} is designated to B–O bond stretching vibrations of BO_4. The band at 1226–1262 cm^{-1} is recognized to asymmetric stretching vibrations of B–O bonds in (BO_3) units (NBO). The peaks at 1302–1357 cm^{-1} explained by asymmetric stretching modes of borate triangles with NBOs. B–O^- stretching vibrations in (BO_3) related to1440 cm^{-1}. The O–H and H_2O bending vibrations in the sample may be responsible for 1534 and 1686 cm^{-1}. The assignments of glass samples are listed in Table 2.

N_4 fraction is defined as $N_4 = \frac{concentrationof(BO4)}{concentrationof(BO4)+concentrationof(BO3)}$ Table 1 shows the N_4 values for each of the glasses examined [46, 47]. The concentration of (BOs) increases with increasing Cr_2O_3 content, according to the Perusal of calculated values for N_4. After Cr_2O_3 is incorporated, BO_3 transforms into BO_4 tetrahedra. The glass network's coherence improves, and the structure stiffens as a result.

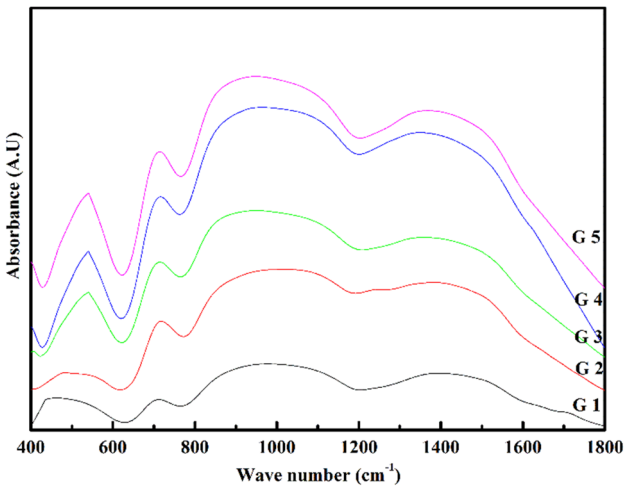

Fig. 3 FT-IR of synthesized glasses

3.3 Optical investigations

In the wavelength range 250–2500 nm, the UV–Vis absorption spectra of Cr_2O_3 doped calcium borosilicate glasses are shown in Fig. 5. In comparison to the G1 glass, the absorption edge of all doped glasses has shifted to a lower wavelength. Figure 6 depicts the absorption coefficient (α) of these glasses. (α) calculated as $\propto = (2.303|d) \times A$. Their intensities have also differed slightly. With Cr_2O_3 doping, the band's absorption intensity has increased. The (Cr^{3+}) is correlated to the identified absorption peaks ranging from 550 to 700 nm.

The determination of the energy $E_{opt.}$ of the glasses is used Tauc's relation: $\alpha h\nu = C(h\nu - E_{opt.})^s$. The relationship between $(\alpha h\nu)^{1/2}$ and $(h\nu)$ is depicted in Fig. 7. Table 3 demonstrates that the $E_{opt.}$ values are in the range of 2.57–3.31 eV [9, 43–50]. According to Babu and Cole, structural changes, and the formation of BOs cause differences in $E_{opt.}$ values. Increases in the $E_{opt.}$ can be linked to density and N_4 variation. Cr-ions occupy interstitial site positions, resulting in increased network compactness and $E_{opt.}$.

Calculating (R_m), ($\propto_m$), (R_L), (χ),M, K_{th} and $T_{g(thero.)}$ using values from the ($E_{opt.}$). The values of (R_m), ($\propto_m$), and (R_L) decrease, although (χ),M increment. Because V_m has decreased, these observations have been reduced. Because the values of ($\propto^\circ$ and $\wedge$) are different, they both decline. The increment in K_{th} and $T_{g(thero.)}$ as Cr_2O_3 is thought to be caused by an increase in the bandgap. Table 3 displays the data values obtained.

(n_D) was determined as $nD = \frac{(1-R)^2+k^2}{(1+R)^2+k^2}$. The investigated sample's n_D increases, as shown in Fig. 8. The relationship between n_D and ρ is similar. As a result, n_D increases as Cr_2O_3, which is thought to be due to a density increase. Calculating R_m, $\propto_0^{2-}$, and Λ using values from the (n_D). The values of R_m, $\propto_0^{2-}$, and Λ are shown in Figs. 9, 10, 11. R_m, $\propto_0^{2-}$, and Λ have the same value as the refractive index.

3.4 Radiation attenuation capacities

Figure 12 shows the (Zeq) value of glass samples. (Zeq) increased then decreased as the incident photon energy was increased and CaO was replaced with Cr_2O_3. This result is due to the Compton scattering interaction. At energies greater than 1 MeV, the (Zeq) value decreases due to the pair creation interaction [22, 48, 51–54].

The variation of EAB and EBAF are presented in Fig. 13. EAF and EABF decrease as the density and Cr_2O_3 in the glasses increase. This also confirms that the photon energy

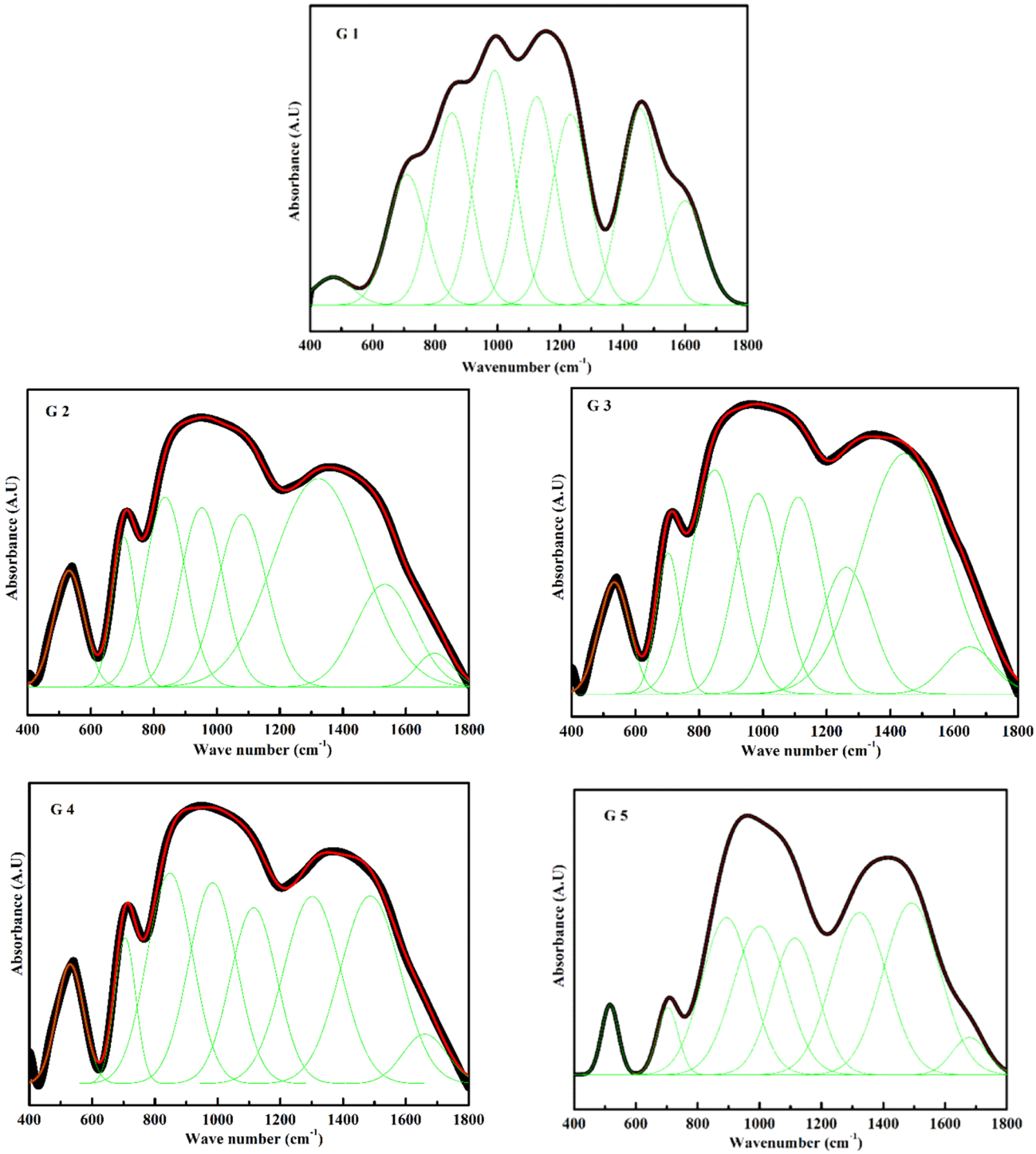

Fig. 4 De-convolution for synthesized glasses

and chemical structure of a material determines its EAF and EABF.

Finally, we use effective removal cross-sections $\sum R$ to investigate the neutron attenuation behaviors of glasses. Figure 14 exemplifies the $\sum R$ of synthesized glasses. As shown in Fig. 15, $\sum R$ is a density-dependent parameter. $\sum R$ enhances as the Cr_2O_3 content of the glasses increases. G 5 is a better fast neutron absorber when the FNRC of glass samples is compared. For neutron attenuation applications, the glass sample G 5 is the best option [22, 48, 51–54].

Table 1 Gaussian fit of synthesized glasses, the band center is (C), and the relative area is (A)

G 1	C	473	–	709	853	990	–	1124	1233	–	1455	–	1600	N4
	A	1.92	–	8.18	14.99	13.3	–	12.25	19.89	–	16.329	–	8.115	0.574
G 2	C	–	507	711	879	–	1021	1118	1226	1356	–	1533		0.578
	A	–	3.768	4.481	21.998	–	12.301	7.759	4.446	29.536	–	15.712		
G 3	C	–	530	705	848	984	–	1115	–	1302	1487	–	1660	0.582
	A	–	5.592	5.351	16.727	16.49	–	14.197	–	18.525	19.447	–	3.672	
G 4	C	–	531	705	836	952	1080	–	–	1322	–	1534	1691	0.592
	A	–	6.144	6.169	13.507	13.475	14.898	–	–	33.161	–	10.583	2.064	
G 5	C	–	516.66	703	893	–	1000	1114	–	1323	1492	–	1679	0.596
	A	–	2.65	4.2	17.3	–	12.7	19.1	–	20.2	15.9	–	2.9	

Table 2 Assignments of FT-IR

Wavenumber, (cm^{-1})	Assignments
~473	Attributed to cationic vibration in the network Cr^{+6}, Ca^{+2}, Na^{+}, and Si^{+4} &Ca–O stretching vibrations in (CaO_6) [6, 8]
~507–531	O–Si–O vibrations overlap with Si–O–B[12, 13]
~703–711	Si–O–Si bending vibrations and B-O-B linkage [12, 13, 43]
~836–879	B–O bonds stretch vibrations of (BO_4) [43, 44]
~1000–1080	Asymmetric stretching vibrations of Si–O–Si, O–Si–O^{-} [5, 45–47]
~952–1118	B–O bonds stretch vibrations in tri-, tetra-, and penta-borate tetrahedral (BO_4) [12, 13]
~1226–1262	B–O bonds asymmetric stretching vibrations of (BO_3) with (NBO) [12, 13, 43–47]
~1302–1357	Asymmetric stretching of borate with NBOs in the pyro-borate [43–47]
~1455–1492	Stretching vibrations of B–O^{-} in (BO_3) [43–47]
~1534	O–H stretching vibrational modes [6, 8, 44]
~1600–1686	H_2O vibrational modes[43]

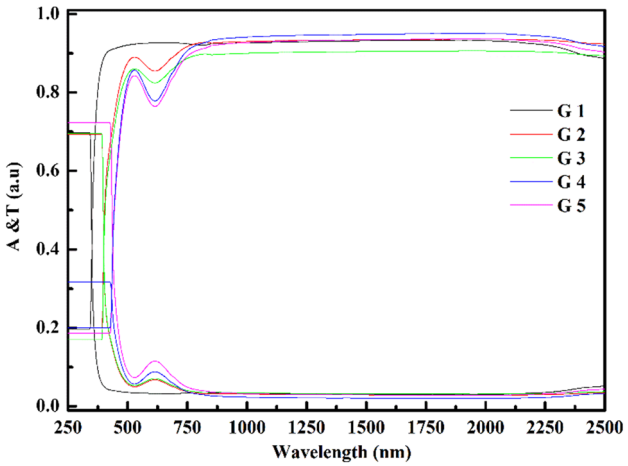

Fig. 5 UV–Vis spectra

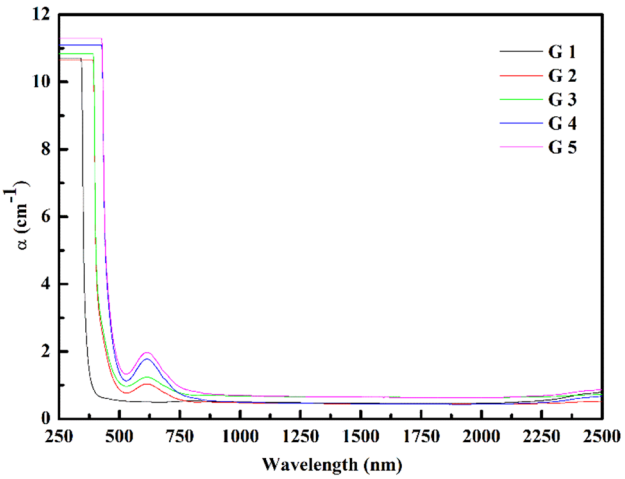

Fig. 6 (α), of fabricated samples

4 Conclusions

Melt quenching was used to successfully fabricate chromium-modified calcium borosilicate glasses. The optical, structural, and γ shielding characteristics of these glasses are investigated. With CrO_6 octahedral structural units, Cr_2O_3 acts as network modifiers. With the addition of Cr_2O_3, the glass density increased while molar volume reduces. All

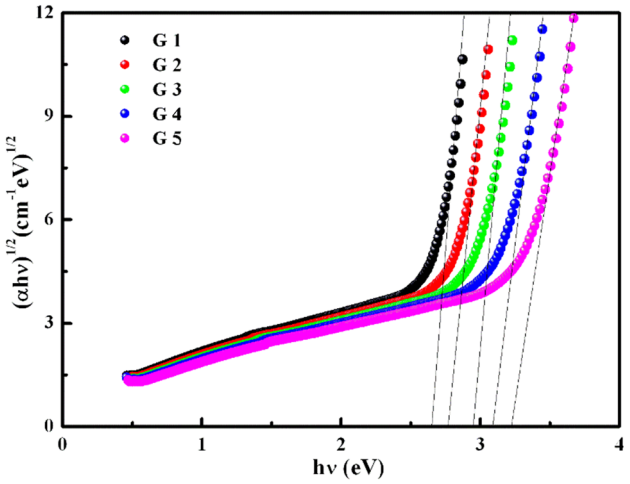

Fig. 7 $(\alpha h\nu)^{1/2}$ against $(h\nu)$ to calculate E_{opt}

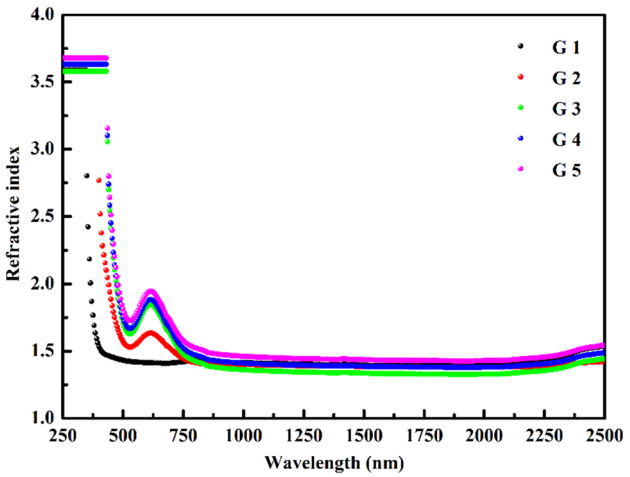

Fig. 8 (n_D), of manufactured samples

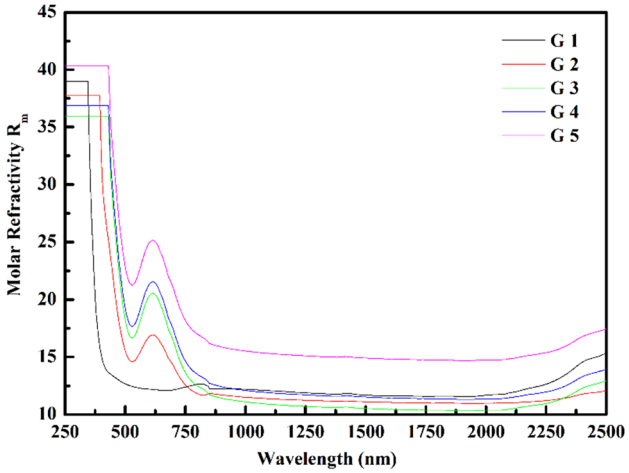

Fig. 9 (R_m), of manufactured samples

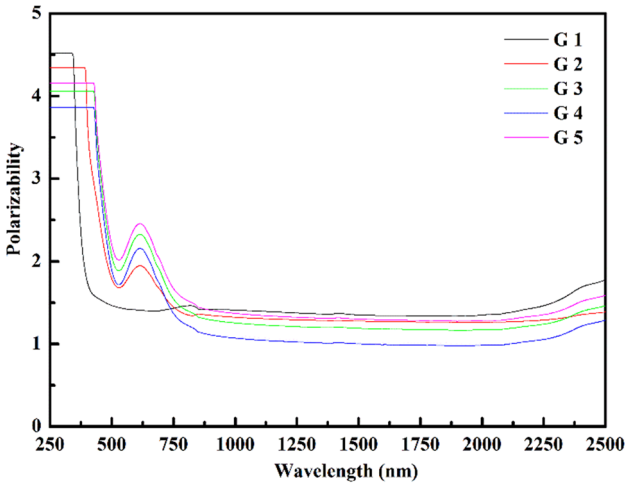

Fig. 10 $(\propto_0^{2-})$, of manufactured samples

Table 3 Optical explanations for glasses

Samples	G 1	G 2	G 3	G 4	G 5
$R_m(cm^3/mol)$	31.06	29.72	28.11	27.15	25.75
$\propto_m(A^{\circ 3})$	12.32	11.79	11.15	10.77	10.21
(R_L)	0.64	0.63	0.62	0.61	0.60
(M)	0.36	0.37	0.38	0.39	0.40
(χ)	0.712	0.744	0.793	0.831	0.8669
(α°)	1.344	1.328	1.303	1.284	1.267
(^)	2.859	2.831	2.786	2.752	2.720
E_{opt}(e.V)	2.65023	2.76724	2.95027	3.09152	3.22524
K_{th}	51.5	74.9	111.5	139.8	166.5
$T_{g(thero.)}$	367.0	414.2	488.1	545.0	599.0

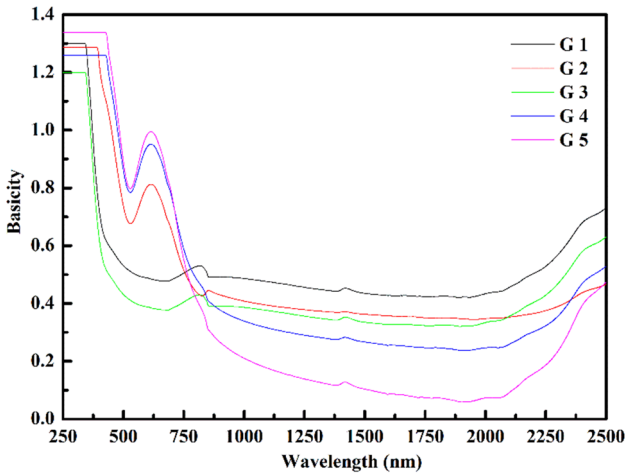

Fig. 11 (Λ), of manufactured samples

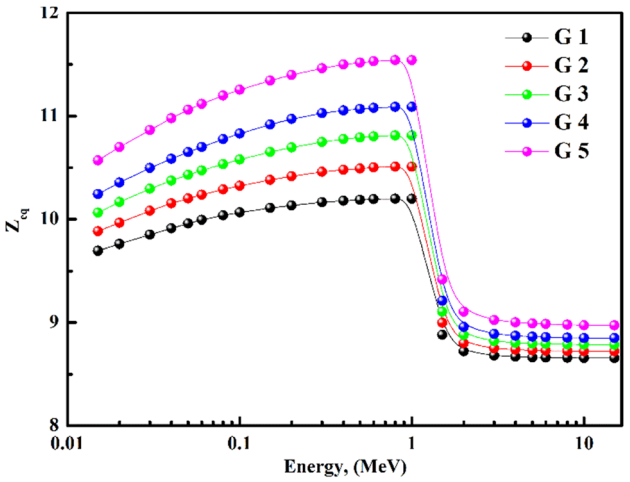

Fig. 12 (*Zeq*) for glasses

glass compositions contain B_2O_3 in the form of BO_3 and BO_4 units, as well as SiO_2 in the SiO_4. The concentration of (BOs) increases with increasing Cr_2O_3 content, according to the Perusal of calculated values for N_4. After Cr_2O_3 is incorporated, BO_3 transforms into BO_4 tetrahedra. The glass network's coherence improves, and the structure stiffens as a result. E_{opt} values are in the range of 2.42–3.18 eV. Increases in the E_{opt} can be linked to density and N_4 variation. (*Zeq*) increased then decreased as the incident photon energy was increased and CaO was replaced with Cr_2O_3. $\sum R$ enhances as the Cr_2O_3 content of the glasses increases. G 5 is a better fast neutron absorber when the FNRC of glass samples is compared. For neutron attenuation applications, the glass sample G 5 is the best option. Incorporating Cr_2O_3 into the investigated glass compositions has a significant impact on their optical, structural, and γ shielding characteristics, according to the findings of this study. This research could

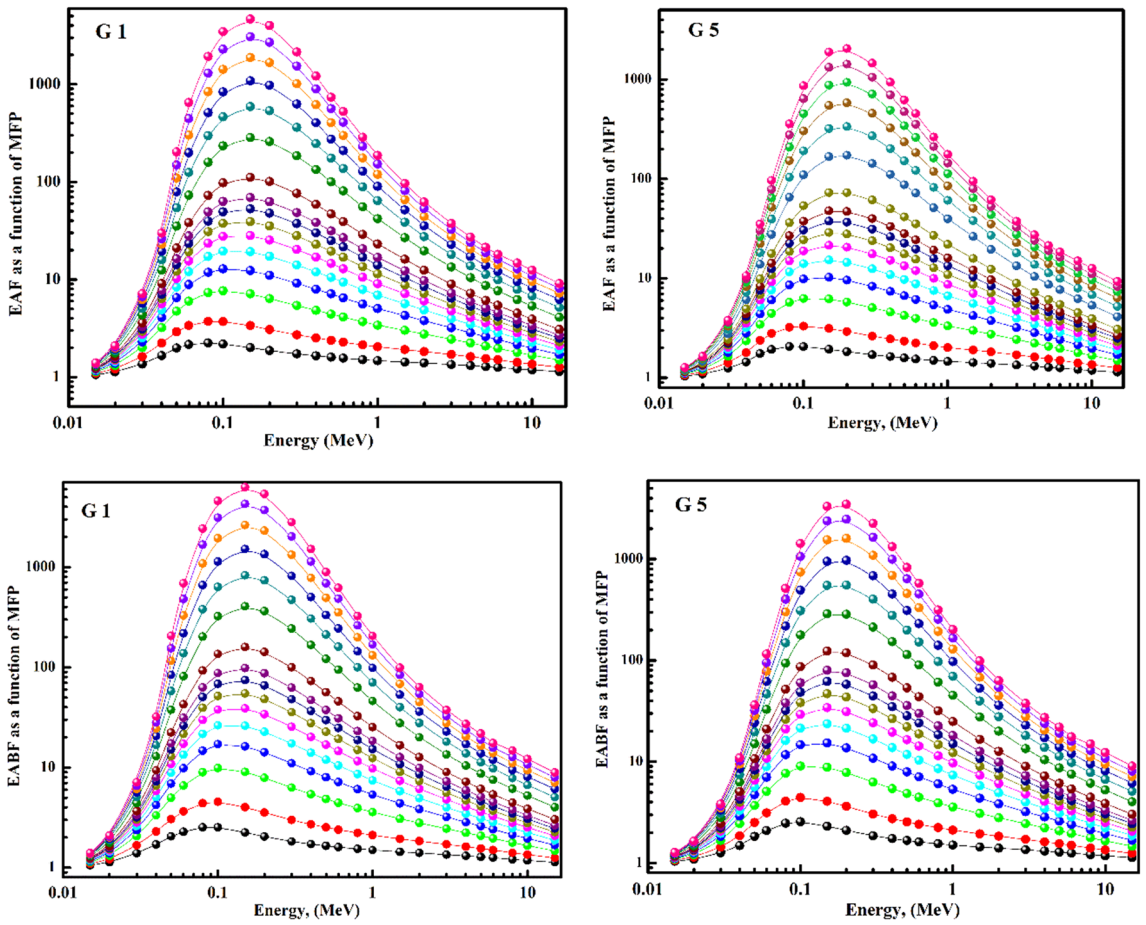

Fig. 13 EAF and EABF for G 1 and G 5 samples

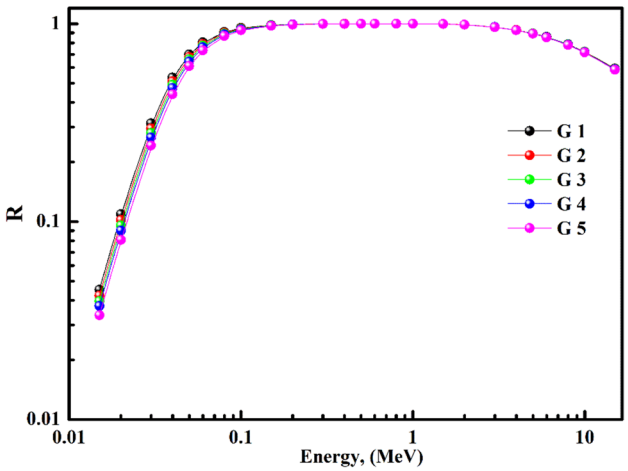

Fig. 14 $\sum R$ for fabricated glasses

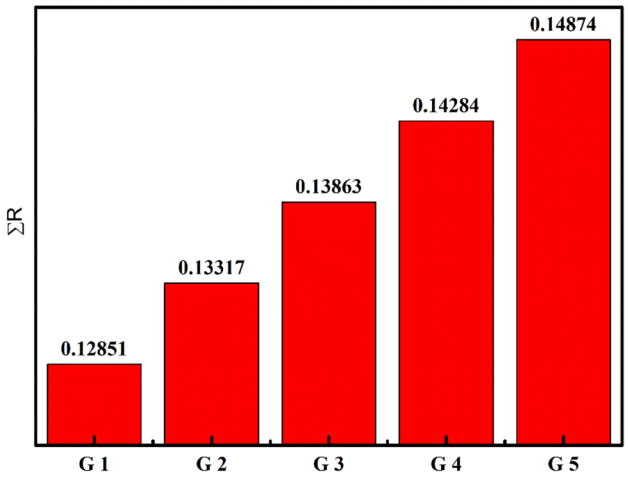

Fig. 15 FNRC with samples

be used in the future to improve optical efficiency and reduce radiation's harmful effects on organisms.s

Acknowledgements We would like to thank Taif University Research Supporting Project number (TURSP-2020/24), Taif University, Taif, Saudi Arabia. Moreover, the authors express their gratitude to the Deanship of Scientific Research at King Khalid University for funding this work through the research groups program under Grant No. R.G.P. 1/298/42.

Author contributions All the authors have given their approval for submission.

Data availability My manuscript and associated personal data.

Declarations

Conflict of interest The authors declare that they have no conflict of interest.

Informed consent The manuscript has not been published elsewhere.

Consent to participate and publication The author's consent to participate and publication.

References

1. M. Kodama, Ultrasonic velocity in sodium borate glasses. J. Mater. Sci. **26**, 4048–4053 (1991). https://doi.org/10.1007/bf02402945
2. M.S.I. Koubisy, K.S. Shaaban, E.A.A. Wahab, M.I. Sayyed, K.A. Mahmoud, Synthesis, structure, mechanical and radiation shielding features of $50SiO_2$–$(48 + X)$ $Na_2B_4O_7$–$(2 - X)$ MnO_2 glasses. Eur. Phys. J. Plus (2021). https://doi.org/10.1140/epjp/s13360-021-01125-4
3. K.H.S. Shaaban, Y.B. Saddeek, K. Aly, Physical properties of pseudo quaternary $Na_2B_4O_7 - SiO_2 - MoO_3 - Dy_2O_3$ glasses. Ceram. Int. **44**, 3862–3867 (2018). https://doi.org/10.1016/j.ceramint.2017.11.175
4. E.A. Abdel Wahab, M.S.I. Koubisy, M.I. Sayyed, K.A. Mahmoud, A.F. Zatsepin, S.A. Makhlouf, K.S. Shaaban, Novel borosilicate glass system: $Na_2B_4O_7$-SiO_2-MnO_2: synthesis, average electronics polarizability, optical basicity, and gamma-ray shielding features. J. Non-Cryst. Solids **553**, 120509 (2021). https://doi.org/10.1016/j.jnoncrysol.2020.120509
5. A. Dahshan, Y.B. Saddeek, K.A. Aly, K.H.S. Shaaban, M.F. Hussein, A.O. Abo El Naga, S.A. Shaban, S.O. Mahmoud, Preparation and characterization of $Li_2B_4O_7 - TiO_2 - SiO_2$ glasses doped with metal-organic framework derived nano-porous Cr_2O_3. J. Non-Cryst. Solids **508**, 51–61 (2019). https://doi.org/10.1016/j.jnoncrysol.2019.01.002
6. K.S. Shaaban, A.M. Al-Baradi, Z.A. Alrowaili, A.M. Ali, M.S. Al-Buriahi, E.A.A. Wahab, Structural, thermal, and mechanical characteristics of yttrium lithium borate glasses and glass–ceramics. J. Mater. Sci.: Mater. Electron. **32**, 28065–28075 (2021). https://doi.org/10.1007/s10854-021-07158-w
7. A.F.A. El-Rehim, H.Y. Zahran, I.S. Yahia, S.A. Makhlouf, K.S. Shaaban, Radiation, crystallization, and physical properties of cadmium borate glasses. SILICON **13**, 2289–2307 (2021). https://doi.org/10.1007/s12633-020-00798-3
8. S. Alomairy, A.M. Aboraia, E.R. Shaaban, K.S. Shaaban, Comparative studies on spectroscopic and crystallization properties of Al_2O_3 -Li_2O- B_2O_3-TiO_2 glasses. Braz. J. Phys. **51**, 1237–1248 (2021). https://doi.org/10.1007/s13538-021-00928-1
9. E.A. Abdel Wahab, K.S. Shaaban, E.S. Yousef, Enhancement of optical and mechanical properties of sodium silicate glasses using zirconia. Opt. Quant. Electron. (2020). https://doi.org/10.1007/s11082-020-02575-3
10. A.F.A. El-Rehim, H.Y. Zahran, I.S. Yahia, A.M. Ali, K.S. Shaaban, Physical, radiation shielding and crystallization properties of Na_2O-Bi_2O_3- MoO_3-B_2O_3- SiO_2-Fe_2O_3 glasses. SILICON (2020). https://doi.org/10.1007/s12633-020-00827-1
11. T. Alharbi, H.F.M. Mohamed, Y.B. Saddeek, A.Y. El-Haseib, K.S. Shaaban, Study of the TiO_2 effect on the heavy metals oxides borosilicate glasses structure using gamma-ray spectroscopy and positron annihilation technique. Radiat. Phys. Chem. **164**, 108345 (2019). https://doi.org/10.1016/j.radphyschem.2019.108345
12. K.S. Shaaban, Y.B. Saddeek, Effect of MoO_3 content on structural, thermal, mechanical and optical properties of (B_2O_3-SiO_2-Bi_2O_3-Na_2O-Fe_2O_3) glass system. SILICON **9**, 785–793 (2017). https://doi.org/10.1007/s12633-017-9558-5
13. K.H. Mahmoud, A.S. Alsubaie, E.A.A. Wahab, F.M. Abdel-Rahim, K.S. Shaaban, Research on the effects of yttrium on

bismuth titanate borosilicate glass system. SILICON (2021). https://doi.org/10.1007/s12633-021-01125-0
14. K.S. Shaaban, I. Boukhris, I. Kebaili, M.S. Al-Buriahi, Spectroscopic and attenuation shielding studies on B_2O_3-SiO_2-LiF-ZnO-TiO_2 glasses. SILICON (2021). https://doi.org/10.1007/s12633-021-01080-w
15. K.S. Shaaban, A.M. Al-Baradi, E.A.A. Wahab, The Impact of Y_2O_3 on physical and optical characteristics, polarizability, optical basicity, and dispersion PARAMETERS of B_2O_3 – SiO_2 – Bi_2O_3 – TiO_2 Glasses. SILICON (2021). https://doi.org/10.1007/s12633-021-01309-8
16. A.M. Al-Baradi, A.F.A. El-Rehim, Z.A. Alrowaili, M.S. Al-Buriahi, K.S. Shaaban, FT-IR and gamma shielding characteristics of 22SiO_2- 23Bi_2O_3-37B_2O_3-13TiO_2-(5–x) LiF- x BaO glasses. SILICON (2021). https://doi.org/10.1007/s12633-021-01481-x
17. A.M. Ali, Z.A. Alrowaili, A.M. Al-Baradi, M.S. Al-Buriahi, E.A.A. Wahab, K.S. Shaaban, A study of thermal, and optical properties of 22SiO_2- 23Bi_2O_3-37B_2O_3-13TiO_2-(5–x) LiF- x BaO glasses. SILICON (2021). https://doi.org/10.1007/s12633-021-01440-6
18. Z.A. Alrowaili, A.M. Al-Baradi, M.A. Sayed, A. Mossad Ali, E.A. Abdel Wahab, M.S. Al-Buriahi, K.S. Shaaban, The impact of Fe_2O_3 on the dispersion parameters and gamma / fast neutron shielding characteristics of lithium borosilicate glasses. Optik (2021). https://doi.org/10.1016/j.ijleo.2021.168259
19. Y.B. Saddeek, K.A. Aly, K.S. Shaaban, A.M. Ali, M.A. Sayed, The Effect of TiO_2 on the optical and mechanical properties of heavy metal oxide borosilicate glasses. SILICON **11**, 1253–1260 (2019). https://doi.org/10.1007/s12633-018-9912-2
20. A.A. El-Maaref, E.A.A. Wahab, K.S. Shaaban, R.M. El-Agmy, Enhancement of spectroscopic parameters of Er^{3+}-doped cadmium lithium gadolinium silicate glasses as an active medium for lasers and optical amplifiers in the NIR-region. Solid State Sci. **113**, 106539 (2021). https://doi.org/10.1016/j.solidstatesciences.2021.106539
21. A.F.A. El-Rehim, K.S. Shaaban, Influence of La_2O_3 content on the structural, mechanical, and radiation-shielding properties of sodium fluoro lead barium borate glasses. J. Mater. Sci.: Mater. Electron. **32**, 4651–4671 (2021). https://doi.org/10.1007/s10854-020-05204-7
22. K.S. Shaaban, S. Alomairy, M.S. Al-Buriahi, Optical, thermal and radiation shielding properties of B_2O_3–NaF–PbO–BaO–La_2O_3 glasses. J. Mater. Sci.: Mater. Electron. (2021). https://doi.org/10.1007/s10854-021-05885-8
23. A.F.A. El-Rehim, A.M. Ali, H.Y. Zahran, I.S. Yahia, K.S. Shaaban, Spectroscopic, structural, thermal, and mechanical properties of B_2O_3-CeO_2-PbO_2 glasses. J. Inorg. Organomet. Polym Mater. **31**, 1774–1786 (2021). https://doi.org/10.1007/s10904-020-01799-w
24. K.S. Shaaban, E.S. Yousef, Optical properties of Bi_2O_3 doped boro tellurite glasses and glass ceramics. Optik **203**, 163976 (2020). https://doi.org/10.1016/j.ijleo.2019.163976
25. M.A. Sayed, A.M. Ali, A.F. Abd El-Rehim et al., Dispersion parameters, polarizability, and basicity of lithium phosphate glasses. J. Elec. Mater. **50**, 3116–3128 (2021). https://doi.org/10.1007/s11664-021-08921-9
26. A.M. Fayad, K.S. Shaaban, W.M. Abd-Allah, M. Ouis, Structural and optical study of CoO doping in borophosphate host glass and effect of gamma irradiation. J. Inorg. Organomet. Polym Mater. **30**, 5042–5052 (2020). https://doi.org/10.1007/s10904-020-01641-3
27. K.S. Shaaban, E.S. Yousef, S.A. Mahmoud, E.A.A. Wahab, E.R. Shaaban, Mechanical, structural and crystallization properties in titanate doped phosphate glasses. J. Inorg. Organomet. Polym Mater. **30**, 4655–4663 (2020). https://doi.org/10.1007/s10904-020-01574-x
28. A.A. El-Maaref, S. Badr, K.S. Shaaban, E.A. Abdel Wahab, M.M. Elokr, Optical properties and radiative rates of Nd^{3+} doped zinc-sodium phosphate glasses. J. Rare Earths **37**, 253–259 (2019). https://doi.org/10.1016/j.jre.2018.06.006
29. E.A. Abdel Wahab, A.A. El-Maaref, K.S. Shaaban, J. Börcsök, M. Abdelawwad, Lithium cadmium phosphate glasses doped Sm^{3+} as a host material for near-IR laser applications. Opt. Mater. **111**, 110638 (2021). https://doi.org/10.1016/j.optmat.2020.110638
30. A. El-Taher, A.M. Ali, Y.B. Saddeek, R. Elsaman, H. Algarni, K. Shaaban, T.Z. Amer, Gamma ray shielding and structural properties of iron alkali alumino-phosphate glasses modified by PbO. Radiat. Phys. Chem. **165**, 108403 (2019). https://doi.org/10.1016/j.radphyschem.2019.108403
31. A. Yadav, M.S. Dahiya, A. Hooda, P. Chand, S. Khasa, Structural influence of mixed transition metal ions on lithium bismuth borate glasses. Solid State Sci. **70**, 54–65 (2017). https://doi.org/10.1016/j.solidstatesciences.2017.06.011
32. K.S. Shaaban, Z.A. Alrowaili, A.M. Al-Baradi, A.M. Ali, E.A.A. Wahab, M.S. Al-Buriahi, Mechanical and thermodynamic characteristics of 22SiO_2- 23Bi_2O_3-37B_2O_3-13TiO_2-(5–x) LiF- x BaO glasses. SILICON (2021). https://doi.org/10.1007/s12633-021-01441-5
33. E. Şakar, Ö.F. Özpolat, B. Alım, M.I. Sayyed, M. Kurudirek, PhyX / PSD: Development of a user-friendly online software for calculation of parameters relevant to radiation shielding and dosimetry. Radiation Phys. Chem. **166**, 108496 (2020). https://doi.org/10.1016/j.radphyschem
34. K.S. Shaaban, E.A. Abdel Wahab, A.A. El-Maaref, M. Abdelawwad, E.R. Shaaban, E.S. Yousef, H. Wilke, H. Hillmer, J. Börcsök, Judd-Ofelt analysis and physical properties of erbium modified cadmium lithium gadolinium silicate glasses. J. Mater. Sci.: Mater. Electron. **31**, 4986–4996 (2020). https://doi.org/10.1007/s10854-020-03065-8
35. K.S. Shaaban, M.S.I. Koubisy, H.Y. Zahran, I.S. Yahia, Spectroscopic properties, electronic polarizability, and optical basicity of titanium-cadmium tellurite glasses doped with different amounts of lanthanum. J. Inorg. Organomet. Polym Mater. **30**, 4999–5008 (2020). https://doi.org/10.1007/s10904-020-01640-4
36. A.A. El-Maaref, R.M. El-Agmy, K.S. Shaaban, E.A. Abdel Wahab, Optical and spectroscopic study of Nd_2O_3-doped SBN glass in the near-infrared, visible and UV regions under pumping up-conversion emissions. Eur. Phys. J. Plus (2021). https://doi.org/10.1140/epjp/s13360-021-01798-x
37. E.A.A. Wahab, A.M. Aboraia, A.M.E. Shafey, K.S. Shaaban, A.V. Soldatov, The effect of ZrO_2 on the linear and non-linear optical properties of sodium silicate glass. Opt. Quant. Electron. (2021). https://doi.org/10.1007/s11082-021-03164-8
38. E.A. Abdel Wahab, K.S. Shaaban, S. Alomairy, M.S. Al-Buriahi, Electronegativity and optical basicity of glasses containing Na/Pb/B and their high performance for radiation applications: role of ZrO_2 nanoparticles. Eur. Phys. J. Plus (2021). https://doi.org/10.1140/epjp/s13360-021-01572-z
39. A.F.A. El-Rehim, K.S. Shaaban, H.Y. Zahran, I.S. Yahia, A.M. Ali, M.M.A. Halaka, S.A. Makhlouf, E.A.A. Wahab, E.R. Shaaban, Structural and mechanical properties of lithium bismuth borate glasses containing molybdenum (lbbm) together with their glass-ceramics. J. Inorg. Organomet. Polym Mater. **31**, 1057–1065 (2021). https://doi.org/10.1007/s10904-020-01708-1
40. A.F.A. El-Rehim, H.Y. Zahran, I.S. Yahia, E.A.A. Wahab, K.S. Shaaban, Structural, elastic moduli, and radiation shielding of SiO_2-TiO_2-La_2O_3-Na_2O glasses containing Y_2O_3. J. Mater. Eng. Perform. **30**, 1872–1884 (2021). https://doi.org/10.1007/s11665-021-05513-w
41. B. Albarzan, A.H. Almuqrin, M.S. Koubisy, E.A. Abdel Wahab, K.A. Mahmoud, Kh.S. Shaaban, M.I. Sayyed, Effect of Fe_2O_3 doping on structural, FTIR and radiation shielding characteristics

of aluminium-lead-borate glasses. Prog. Nucl. Energy **141**, 103931 (2021). https://doi.org/10.1016/j.pnucene.2021.103931
42. S. Alomairy, M.S. Al-Buriahi, E.A. Abdel Wahab, C. Sriwunkum, K. Shaaban, Synthesis, FTIR, and neutron/charged particle transmission properties of Pb_3O_4–SiO_2–ZnO–WO_3 glass system. Ceram. Int. **47**, 17322–17330 (2021). https://doi.org/10.1016/j.ceramint.2021.03.045
43. M. Bala, S. Agrohiya, S. Dahiya, A. Ohlan, R. Punia, A.S. Maan, Effect of replacement of Bi_2O_3 by Li_2O on structural, thermal, optical and other physical properties of zinc borate glasses. J. Mol. Struct. **1219**, 128589 (2020). https://doi.org/10.1016/j.molstruc.2020.128589
44. S. Bale, N.S. Rao, S. Rahman, Spectroscopic studies of Bi_2O_3–Li_2O–ZnO–B_2O_3 glasses. Solid State Sci. **10**, 326–331 (2008). https://doi.org/10.1016/j.solidstatesciences.2007.09.017
45. M. Hubert, A.J. Faber, On the structural role of boron in borosilicate glasses. Eur. J. Glass Sci. Technol. Part B Phys. Chem. Glasses **55**(3), 136–158 (2014)
46. M.S. Gaafar, S.Y. Marzouk, Mechanical and structural studies on sodium borosilicate glasses doped with Er_2O_3 using ultrasonic velocity and FTIR spectroscopy. Physica B **388**(1–2), 294–302 (2007). https://doi.org/10.1016/j.physb.2006.06.132
47. T. Walia, K. Singh, Mixed alkaline earth modifiers effect on thermal, optical and structural properties of SrO-BaO-SiO_2-B_2O_3-ZrO_2 glass sealants. J. Non-Cryst. Solids **564**, 120812 (2021). https://doi.org/10.1016/j.jnoncrysol.2021.120812
48. E.A. Abdel Wahab, K.S. Shaaban, Structural and optical features of aluminum lead borate glass doped with Fe_2O_3. Appl. Phys. A (2021). https://doi.org/10.1007/s00339-021-05062-y
49. K.S. Shaaban, A.M. Al-Baradi, A.M. Ali, Investigation of BaO reinforced TiO_2–P_2O_5–li_2O glasses for optical and neutron shielding applications. RSC Adv. **12**, 3036–3043 (2022). https://doi.org/10.1039/d2ra00171c
50. E.A.A. Wahab, K.S. Shaaban, A.M. Al-Baradi, Enhancement of optical and physical parameters of lead zinc silicate glasses by doping W^{+3} ions. SILICON (2021). https://doi.org/10.1007/s12633-021-01236-8
51. M.A. Alothman, Z.A. Alrowaili, J.S. Alzahrani, E.A.A. Wahab, I.O. Olarinoye, C. Sriwunkum, K.S. Shaaban, M.S. Al-Buriahi, Significant influence of MoO_3 content on synthesis, mechanical, and radiation shielding properties of B_2O_3-Pb_3O_4-Al_2O_3 glasses. J. Alloy. Compd. **882**, 160625 (2021). https://doi.org/10.1016/j.jallcom.2021.160625
52. S. Alomairy, Z.A. Alrowaili, I. Kebaili, E.A.A. Wahab, C. Mutuwong, M.S. Al-Buriahi, K.S. Shaaban, Synthesis of Pb_3O_4-SiO_2-ZnO-WO_3 glasses and their fundamental properties for gamma shielding applications. SILICON (2021). https://doi.org/10.1007/s12633-021-01347-2
53. M.H.A. Mhareb, M.I. Sayyed, Y.S.M. Alajerami, M. Alqahtani, N. Dwaikat, A.M. Alsagry, M. Al-Yatimi, M. Zakariah, Structural and radiation shielding features for a new series of borate glass samples: part I. Eur. Phys. J. Plus (2021). https://doi.org/10.1140/epjp/s13360-020-00984-7
54. Y.B. Saddeek, K.H.S. Shaaban, R. Elsaman, A. El-Taher, T.Z. Amer, Attenuation-density anomalous relationship of lead alkali borosilicate glasses. Radiat. Phys. Chem. **150**, 182–188 (2018). https://doi.org/10.1016/j.radphyschem.2018.04.028